Discovery of a possibly old galaxy at $z = 6.027$, multiply imaged by the massive cluster Abell 383

Johan Richard[1,2]⋆, Jean-Paul Kneib[3], Harald Ebeling[4], Daniel P. Stark[5], Eiichi Egami[6], Andrew K. Fiedler[6]

[1] *CRAL, Observatoire de Lyon, Université Lyon 1, 9 Avenue Ch. André, 69561 Saint Genis Laval Cedex, France*
[2] *Dark Cosmology Centre, Niels Bohr Institute, University of Copenhagen, Juliane Maries Vej 30, DK-2100 Copenhagen, Denmark*
[3] *Laboratoire d'Astrophysique de Marseille, CNRS- Université Aix-Marseille, 38 rue F. Joliot-Curie, 13388 Marseille Cedex 13, France*
[4] *Institute of Astronomy, University of Hawaii, Honolulu, HI 96822, USA*
[5] *Institute of Astronomy, University of Cambridge, Madingley Road, Cambridge CB3 0HA, UK*
[6] *Steward Observatory, University of Arizona, 933 N. Cherry Avenue, Tucson, AZ 85721, USA*

ABSTRACT

We report the discovery of a unique $z = 6.027$ galaxy, multiply imaged by the cluster Abell 383 and detected in new *Hubble Space Telescope* ACS and WFC3 imaging, as well as in *Warm Spitzer* observations. This galaxy was selected as a pair of i-dropouts; its suspected high redshift was confirmed by the measurement of a strong Lyman-α line in both images using Keck/DEIMOS. Combining *Hubble* and *Spitzer* photometry after correcting for contamination by line emission (estimated to be a small effect), we identify a strong Balmer break of 1.5 magnitudes. Taking into account the magnification factor of 11.4 ± 1.9 (2.65 ± 0.17 mag) for the brightest image, the unlensed AB magnitude for the source is 27.2 ± 0.05 in the H band, corresponding to a 0.4 L* galaxy, and 25.7 ± 0.08 at 3.6 μm. The UV slope is consistent with $\beta \sim 2.0$, and from the rest-frame UV continuum we measure a current star formation rate of 2.4 ± 1.1 M$_\odot$/yr. The unlensed half-light radius is measured to be 300 pc, from which we deduce a star-forming surface density of ~ 10 M$_\odot$ yr^{-1} kpc^{-2}. The Lyman-α emission is found to be extended over $\sim 3''$ along the slit, corresponding to ~ 5 kpc in the source plane. This can be explained by the presence of a much larger envelope of neutral hydrogen around the star-forming region. Finally, fitting the spectral energy distribution using 7 photometric data points with simple SED models, we derive the following properties: very little reddening, an inferred stellar mass of $M^* = 6~10^9$ M$_\odot$, and an inferred age of ~ 800 Myrs (corresponding to a redshift of formation of ~ 18). The star-formation rate of this object was likely much stronger in the past than at the time of observation, suggesting that we may be missing a fraction of galaxies at z$\sim$6 which have already faded in rest-frame UV wavelengths.

Key words: galaxies: high redshift - gravitational lensing: strong

1 INTRODUCTION

One of the most important topics of modern cosmology is the nature of the sources that reionized the intergalactic medium in the early Universe. A lot of progress has been made in characterizing the bright end of the population of high-redshift galaxies through the selection of *optical dropouts* using both space- and ground-based data (e.g. Bouwens et al. 2006; McLure et al. 2010). In particular, the

luminosity function of galaxies at $z \sim 6$ is well constrained down to 0.1 L* thanks to very deep observations of fields such as GOODS and the Hubble Ultra Deep Field (UDF), which provided over 500 i-dropouts (Bouwens et al. 2006, 2007).

Solely based on photometric selection, the observed trend implies highly significant evolution at the bright end of the luminosity function ($> L^*$) between $z \sim 4$ and $z \sim 7$, with a large decrease in the number of luminous sources. If this trend extends to higher redshifts, there might not be a sufficient number of ionizing photons to explain the observed

⋆ E-mail: johan.richard@univ-lyon1.fr

change of the intergalactic medium. One possible solution to this problem would be the presence of a high number of low-mass/low-luminosity sources at these redshifts, which would contribute to the bulk of the ionizing radiation. However, only a small fraction of the currently known dropouts at $z \sim 6$ have luminosities of 0.1-0.5L^* (L^* corresponds to $\sim$26.3 AB at $z \sim 6$), and even fewer are spectroscopically confirmed (Stark et al. 2010, 2011).

The newly installed Wide Field Camera 3 (WFC3) on-board the *Hubble Space Telescope* (HST) enables deep near-infrared imaging that is very fast compared to any other instrument. So far most of the high-redshift work using WFC3 has been performed on deep fields, the UDF in particular, and numerous and convincing candidates for galaxies at redshifts $z \sim 7$ (McLure et al. 2010; Bunker et al. 2010; Finkelstein et al. 2010) or even $z \sim 10$ (Bouwens et al. 2011) have been identified. However, the typical magnitudes of these objects ($\sim$27-28, and ~ 29 for the $z \sim 10$ candidate) make ground-based spectroscopy challenging. Combining WFC3 and the *Spitzer Space Telescope* (SST) at longer wavelengths allows us to study the star-formation history of these high-redshift galaxies, and to derive constraints on the age of the stellar population and the total stellar mass, thanks to the high sensitivity of the first two IRAC channels (e.g., Egami et al. 2005). In particular, Stark et al. (2009) measured the masses of optical dropouts from $z \sim 4$ and $z \sim 6$, and found no significant evolution in the ratios of stellar mass to UV light. However, ages and stellar masses are best constrained in the brightest IRAC detections and quite uncertain for faint objects.

A complementary and very powerful approach is to observe the high-redshift Universe through massive cluster lenses. Gravitational lensing offers the opportunity to perform high signal-to-noise observations of galaxies that would otherwise be too faint and distant for quantitative study. Although the intrinsic lensed volume probed by any individual cluster observation is small compared to its unlensed equivalent, gravitational amplification by clusters likely represents a unique way to perform ground-based spectroscopy of objects that are intrinsically as faint as mag$\sim$30 (Ellis et al. 2001; Kneib et al. 2004; Richard et al. 2008).

Combining the resolution and sensitivity of the Wide-Field Camera 3 (WFC3) and the Advanced Camera for Surveys (ACS) with the magnification afforded by clusters used as *gravitational telescopes* the recently approved Multi-Cycle Treasury "CLASH" cluster program on HST (PI: Postman; 25 clusters; 524 orbits) offers a fresh opportunity to find and study high-redshift galaxies. Two thirds of the CLASH clusters have also been observed with SST/IRAC as part of our SST Warm Mission Exploratory Science program, "The IRAC Lensing Survey" (PI: Egami; 53 clusters; 593 hours), which obtains deep (5 hours/band) images in the two shorter-wavelength IRAC channels (3.6 and 4.5μm). Together, these two large HST and SST observing programs facilitate a detailed study of the physical properties of distant lensed galaxies.

In this letter, we report the discovery of a high-redshift *i*-dropout in Abell 383 (ID 12065), which we confirmed to be at $z = 6.027$ based on Keck spectroscopy. We summarize the observations performed in Section 2 and present results of our photometric and spectroscopic analysis in Section 3. Conclusions are given in Section 4. Magnitudes are quoted

in the AB system. At $z = 6$, $1''$ on the sky corresponds to a projected distance of 5.710 kpc in the adopted cosmology ($\Omega_m = 0.3$, $\Omega_\Lambda = 0.7$, $h = 0.7$).

2   IMAGING AND SPECTROSCOPY

HST images of the core of the massive galaxy cluster Abell 383 (α=02:48:03.332, δ=-03:31:44.98,z =0.187) have been obtained with ACS and WFC3/IR between November 2010 and February 2011 in 10 filters from optical to near-infrared (F435W, F475W, F606W, F625W, F775W, F814W, F850LP, F110W, F125W, F160W) with exposure times of 2000-3000 s per band. Individual ACS frames were corrected for charge transfer efficiency following the procedure described by Massey (2010), adjusted to correct the most recent ACS images (more details will be given in Paraficz et al. in prep.). We measured the relative shifts between different epochs of observations in a given filter and combined the ACS and WFC3 with multidrizzle (Koekemoer et al. 2002) to obtain the final images.

We then performed a search for *i* dropouts meeting the colour criteria F775W-F850LP> 1.3 (Bouwens et al. 2006) in the strong-lensing region of the cluster. The envelope of the Brightest Cluster Galaxy (BCG) has been subtracted beforehand, using an elliptical surface-brightness model constructed with the IRAF task ELLIPSE following the technique presented in Richard et al. (2008). This model provides a good subtraction overall, except for residuals at the very centre that are due to the presence of a compact source and a dust lane, features already pointed out by Smith et al. (2005). We used SExtractor (Bertin & Arnouts 1996) in *double-image* mode to obtain photometry across all HST bands. The F110W (most sensitive observation) was used as a *detection* image and the other bands as *measurement* images. Colours were measured between two bands inside the same 0.3$''$ aperture and scaled to match the total magnitude in the F110W band (MAG_AUTO with an isophote of $\sim 0.6''$ diameter). We used a 3-σ upper limit for the photometry in case of non-detections.

We identified two *i*-dropouts located $10''$ north (image 5.1: α=02:48:03.264, δ=-03:31:34.77) and $25''$ southeast (image 5.2: α=02:48:04.600,δ=-03:31:58.47) of the BCG (Fig. 1). They show a strong continuum break (F775W-F850LP > 1.9 mag.) and their colours agree within each other to better than the 1σ error. The background gradient around image 5.1 is efficiently removed and the increased sky noise is estimated locally by SExtractor. The measurements of both images are listed in Table 1. Our well constrained lensing model for the mass distribution in this cluster (see Section 3) predicts that both images 5.1 and 5.2 are associated with the same source (referred to as source 5), when assuming a redshift $z > 5.5$.

On January 3, 2011 we used the DEep Imaging Multi-Object Spectrograph (DEIMOS) on the Keck II telescope to obtain an optical spectrum with a 1.2$''$-wide slit aligned to cover both images (Fig. 1). Aiming to detect Lyman-α emission from this source, we used the red-efficient 600ZD grating for three exposures of 1800 s. The reduction of the resulting data was performed with standard IRAF routines for bias subtraction, flat-fielding, sky subtraction and wavelength calibration. The standard star Feige 110 observed

Image	F775W	F814W	F850LP	F110W	F125W	F160W	$3.6\mu m$	$4.5\mu m$
5.1	> 26.48	25.63±0.14	24.54±0.12	24.65±0.05	24.57±0.08	24.66±0.05	23.10±0.08	22.91±0.08
5.2	> 26.48	26.41±0.23	25.35±0.21	25.16±0.08	25.18±0.08	25.15±0.07	N/A	N/A

Table 1. Summary of the measured photometry for both images.
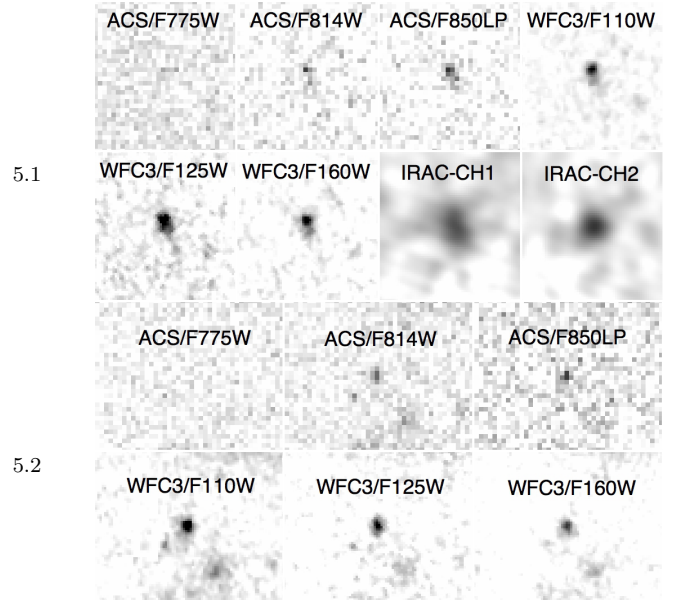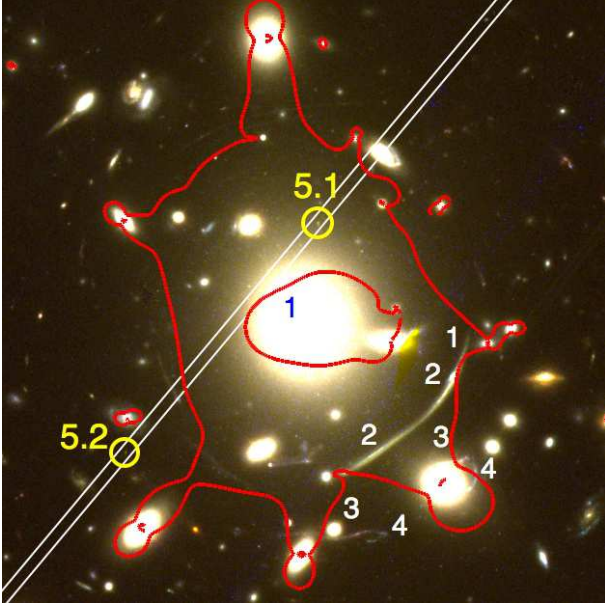
Figure 1. Left: F814W-F110W-F160W colour image of the very core of Abell 383, together with known multiply-imaged systems (marked 1 to 5) and the critical line at $z = 6$. The identified i-dropout is seen as two images marked by yellow circles; the DEIMOS long-slit used in our spectroscopic follow-up is shown in white. Right: postage stamps of both images. HST and IRAC images are $3''$ and $6''$ a side, respectively.

during the same night was used for flux calibration. Seeing was $1.1''$ and conditions photometric.

A strong emission line is detected at 8545 Å at the locations of both images in the sky-subtracted spectrum (Fig. 2). We measure an integrated flux of $2.2 \pm 0.3\ 10^{-17}$ erg s^{-1} cm^{-2} in the extracted 1D spectrum of the brightest image (5.1) and a spatial extent of $\sim 3''$, much larger than the seeing of the observations. The line profile shows a possible asymmetry, but due to the close proximity of a skyline the signal-to-noise is too poor for an accurate measurement of the profile on the red side. However, all available evidence (including the lensing configuration and photometry) support the identification of this line as Lyman-α at a redshift $z_{\rm spec} = 6.027 \pm 0.002$ (measured at the peak of the line).

In addition to the HST images, we used the SST/IRAC data of Abell 383 obtained at three different epochs (August 2005, September 2009, March 2010). The first data set was obtained by programme 83 (PI: G. Rieke) for a total integration time of 40 minutes/band. The second and third data sets were obtain by programme 60034 (PI: E. Egami; "The IRAC Lensing Survey") and yielded a total 2-epoch integration time of 5 hours/band. The Basic Calibrated Data (BCD) frames were mosaicked using MOPEX (MOsaicker and Point source EXtractor), a software package distributed by the *Spitzer Science Center*, using a pixel scale of $0.''6$ (half of the original instrumental pixel scale).

Images 5.1 and 5.2 are detected in the two first IRAC channels ($3.6\mu m$ and $4.5\mu m$). We used a model of the BCG convolved with the IRAC point-spread function (PSF) to

subtract its contribution and used a larger aperture ($2''$) to measure the colour between the WFC3/F110W band and the IRAC bands. Using a $1''$ aperture (more similar to the isophote used to infer the total magnitude) gives consistent colours but higher error bars. The WFC3 and IRAC images were convolved with an empirical IRAC PSF and a TINYTIM (Hook & Stoehr 2008) model of the WFC3 PSF, respectively. We checked this photometry matching between HST and SST using cluster members as well as background sources of known spectroscopic redshift. Again, the photometry for image 5.1 (scaled to the total magnitude in F110W) is listed in Table 1. IRAC colours were not measured for image 5.2 since we were unable to remove the contamination from nearby non-elliptical cluster members. As the observed IRAC colours are entirely consistent between the 3 epochs, the BCG contribution to the sky noise is within the measured errors. We adopt an average of the values from the two best epochs (2 and 3).

3 PHYSICAL PROPERTIES

We now estimate the strong-lensing magnification factors of images 5.1 and 5.2 based on a parametric model for the mass distribution of the cluster core. This model is constructed using LENSTOOL[1] (Jullo et al. 2007), and based on a similar model constrained by 4 multiply imaged systems (referred

---

[1] http://lamwws.oamp.fr/lenstool/
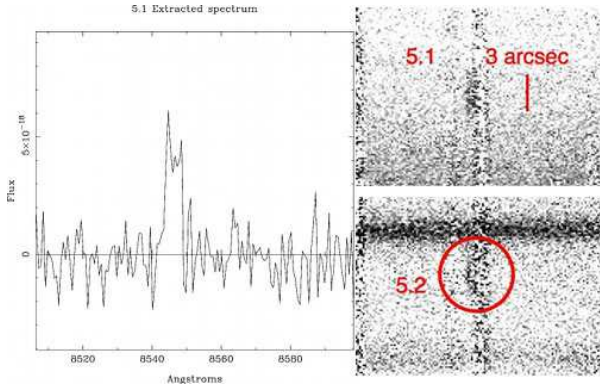
Figure 2. 2D long-slit spectrum as obtained with Keck/DEIMOS, covering both images 5.1 and 5.2 and showing a clear emission line at 8545 Å for both 5.1 and 5.2. The inset presents the extracted spectrum of image 5.1 around this wavelength.

to as systems 1 to 4, Fig. 1) presented previously by Smith et al. (2003) and Richard et al. (2010). Pseudo-isothermal elliptical mass distributions are used for both the cluster-scale component and individual galaxies. We include in our optimisation the recent spectroscopic redshifts obtained by Newman et al. (2011) for systems 3 and 4. The location of the new pair of images identified in this letter (5.1 / 5.2) is in excellent agreement (within $0.5''$) with the predictions from this model at $z = 6$. We therefore use this new information as an additional constraint (system 5) to improve the mass model. From the family of best models resulting from the optimisation, we derive a magnification factor $\mu_1 = 11.4 \pm 1.9$ and $\mu_2 = 7.3 \pm 1.2$ for images 5.1 and 5.2, respectively. The ratio μ_1/μ_2 is in perfect agreement with the F110W photometry. A third image (5.3) is predicted but is demagnified and located at the very centre of the BCG, making its detection extremely challenging, if not impossible.

Taking into account these magnification factors, we derive intrinsic properties for the original background source 5. Its unlensed F110W (J band) magnitude (27.4 AB) corresponds to an $\sim 0.4L^*$ galaxy at $z = 6$, which makes it more representative of the galaxy population at this redshift than brighter objects, such as the i-dropout identified in Abell 1703 (Richard et al. 2009) which corresponds to a $\sim 3.6L^*$ galaxy. A particularly interesting feature of source 5 is the large magnitude break $(1.50 \pm 0.10$ mag) between the H band (F160W) and the two first channels of IRAC, pass-bands that straddle the location of the rest-frame Balmer break. In order to interpret the implications of this break for the properties of the underlying stellar populations, we performed a Spectral Energy Distribution (SED) fit of image 5.1 (highest S/N image) with a library of spectral templates following the precepts discussed in detail by Stark et al. (2009). The main parameters we aim to derive are the total stellar mass (M*), the current star-formation rate (SFR) and the age of the stellar population (T). To this end, we removed the contribution of the measured Lyman-α line in the F814W and F850LP photometry, and then fit Charlot & Bruzual(2007, S. Charlot, private communication) stellar-population synthesis models to the observed SEDs. We considered exponentially decaying star formation histories of the form SFR(t) $\simeq \exp(-t/\tau)$ with e-folding times of $\tau = 10$,

70, 100, 300, and 500 Myr, in addition to models with continuous star formation (CSF). T is restricted to the range of 10 to 1000 Myr (the age of the universe at $z \sim 6$). We use a Salpeter initial mass function (IMF) (Salpeter 1955) and the dust extinction law of Calzetti et al. (2000) with $0.0 < E(B-V) < 1.0$. Finally, we allow the metallicity to vary between solar (Z$_\odot$) and 0.2 Z$_\odot$, but note that metallicity is degenerate with reddening and has a second-order effect on the SED. Absorption by the intergalactic medium is accounted for following Meiksin (2006).

We next consider the possibility that the strong break between the H band and the IRAC channels is due to contamination by nebular emission lines. Strong Hα, Hβ and [OIII] lines would all fall into the IRAC bands and could boost the continuum, mimicking a stronger Balmer break (Schaerer & de Barros 2010). We correct for this effect as follows: the SFR estimated from SED fitting is consistent with the observed Lyman-α flux, when assuming an aperture correction of a factor of 2 and (conservatively) 1/3 case B for Lyman-α. We predict observed fluxes $f_{H\alpha} = 1.46 \ 10^{-17}$, $f_{H\beta} = 5.1 \ 10^{-18}$ and $f_{[OIII]} = 6.7 \ 10^{-18}$ (cgs units, both [OIII] lines average from COSMOS galaxies, Zoubian et al. 2011 in prep.). We therefore lower the fluxes by 0.06 and 0.04 magnitudes at 3.6 μm and 4.5μm, respectively, thereby eliminating contamination from unresolved line emission. This correction is negligible and we observe no significant change in the best-fit model using this updated photometry.

The observed SED and the best-fitting template are presented in Fig. 3. The best fit is achieved for a $\tau = 500$ Myr star-formation history. The full set of templates gives an age range of T=640-940 Myrs (within a $\Delta\chi^2 = 3$ from the best model), depending on the exact star-formation history, corresponding to a redshift of formation of $z_f = 18 \pm 4$. More punctuated star-formation histories ($\tau = 10 - 100$ Myrs) could produce similar Balmer breaks with ages of only $T = 130 - 300$ Myrs, but they produce much poorer fits to the data ($\Delta\chi^2 \sim 50$, Fig. 3). However, we acknowledge these are simple models and age-dependent dust extinction (Poggianti et al. 2001) as well as more complex star-formation histories (two-component models, with bursts on top of a continuous star-formation) could provide younger ages. This would affect the inferred ages more strongly than the inferred stellar masses, which are more independent of the assumed star-formation history. The most precise measurement is the rest-frame V-band luminosity of $2.2^{+0.97}_{-0.42} \ 10^{10}$ L$_\odot$. The inferred values from the best fit model are a stellar mass of M*=$6.3^{+2.8}_{-1.2} \ 10^9$ M$_\odot$, current SFR of 3.2 ± 1.1 M$_\odot$/yr, and specific SFR ($SSFR = SFR/M^*$, e.g. Brinchmann et al. 2004) of $\sim 5 \ 10^{-10}$ yr^{-1} indicate relatively vigorous star formation similar to the one found by Egami et al. (2005). Note that the relative error in the magnification factor has been added in quadrature for all intrinsic values. The rest-frame UV photometry, around 1500 Å, is consistent with a model of constant AB magnitude, or equivalently with a slope of $\beta \sim 2$ (defined as $f_\lambda \propto \lambda^{-\beta}$). This is consistent with the very small amount of dust (E(B-V)< 0.06) in the best-fit model, and also with the results found for $z \sim 7$ dropouts in the UDF (Bouwens et al. 2010).

Interestingly, image 5.1 of the galaxy is well resolved in the WFC3/F110W image, as an ellipse of size $\sim 0.55'' \times 0.3''$ based on well detected pixels. We measure a half-light radius $r_h = 0.21''$ with SEXTRACTOR, correspond-
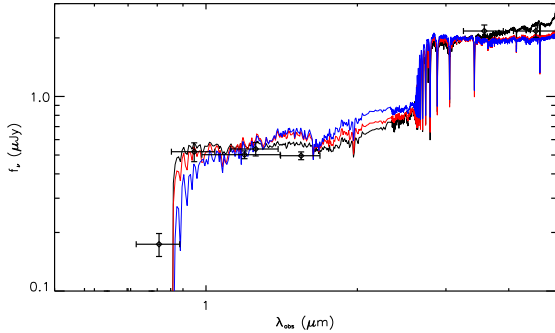
Figure 3. Observed SED of image 5.1 (black data points) and model templates. The black curve represents the best fit to the photometry ($\tau = 500$ Myrs), whereas the blue/red curves show the best fit for younger but more punctuated star-formation histories ($\tau = 10/100$ Myrs respectively), giving a poorer fit to the photometry.

ing to a source-plane radius of $0.06''$, or 0.3 kpc after correcting for the PSF contribution. In comparison, the $3''$ extent of Lyman-α emission observed with DEIMOS, at least in the direction of the slit orientation, corresponds to a 5 kpc diameter in the source plane. This discrepancy consititutes strong evidence for the presence of a large envelope of neutral hydrogen surrounding the star-forming region responsible for the UV emission (Steidel et al. 2011). Of course, as these size measurements are given in UV rest-frame, it is quite likely that the source is imbedded in a lower surface- brightness halo, and the low reddening inferred would be coming from the UV-bright component. Nevertheless, a possible $3''$ diameter dusty component would have been resolved with IRAC.

4 AN EVOLVED GALAXY IN A YOUNG UNIVERSE ?

Taken at face value, the presence of a large optical break and an inferred mature stellar population ($\sim$800 Myrs) only 1 Gyr after the Big Bang is challenging. As previously discussed, this value depends on the assumptions made in the standard models of star-formation history used. Mobasher et al. (2005) reported a similarly strong Balmer break for a brighter and more massive galaxy at $z \sim 6.5$, which, however, still lacks spectroscopic confirmation despite numerous attempts. If we compare the intrinsic (i.e., demagnified) properties of this lensed galaxy with those of the 16 i-dropouts with spectroscopic redshifts analysed by Eyles et al. (2007) and fit with similar SED models, this galaxy is 1 magnitude fainter in rest-frame UV ($F850LP = 27.4$) but has a similar flux redward of the Balmer break (although with a much stronger detection thanks to its magnification by the cluster lens) and therefore the same typical mass. The small size of the star-forming region implies a star-formation surface density of $\sim$10 M$_\odot$ yr^{-1} kpc^{-2}, comparable to the most intense starburst activity observed locally (Kennicutt 1998) and allowing this object to drive strong winds.

The detection of a large Balmer break, at such a high significance, is quite remarkable and demonstrates that subluminous systems (when selected in the UV) may not always

be observed at a young stage of evolution. This is consistent with results obtained from IRAC stacking of faint $z = 6 - 7$ field galaxies (Stark et al. 2009; Labbé et al. 2010), and 15% of the Stark et al. (2009) sample of bright i-dropouts show similar Balmer breaks. Thanks to the magnification provided by gravitational lensing, we can measure this feature in faint individual objects. This result is important both for estimating the mass function at high redshift, and even more for understanding the process of reionisation, as it implies a significant contribution at $z > 10$ from the progenitors of these objects.

From our knowledge of the UV luminosity function at $z \sim 6$ (Bouwens et al. 2006), we expect ~ 0.5 objects of this kind per CLASH cluster in the strong-lensing (multiply imaged) regime down to 0.2 L*. Deeper WFC3 and ACS observations of strong-lensing clusters would efficiently make use of the *Spitzer Warm mission* program and allow us to measure the distribution of Balmer breaks in a larger sample down to even fainter magnitudes, and thus to precisely determine the mass function.

REFERENCES

Bertin E., Arnouts S., 1996, A&AS, 117, 393

Bouwens R. J., Illingworth G. D., Blakeslee J. P., Franx M., 2006, ApJ, 653, 53

Bouwens R. J., Illingworth G. D., Franx M., Ford H., 2007, ApJ, 670, 928

Bouwens R. J., Illingworth G. D., Labbe I., Oesch P. A., Trenti M., Carollo C. M., van Dokkum P. G., Franx M., et al., 2011, Nature, 469, 504

Bouwens R. J., Illingworth G. D., Oesch P. A., Trenti M., Stiavelli M., Carollo C. M., Franx M., van Dokkum P. G., Labbé I., Magee D., 2010, ApJ, 708, L69

Brinchmann J., Charlot S., White S., Tremonti C., Kauffmann G., Heckman T., Brinkmann J., 2004, MNRAS, 351, 1151

Bunker A., Wilkins S., Ellis R., Stark D., Lorenzoni S., Chiu K., Lacy M., Jarvis M., Hickey S., 2010, MNRAS, 409, 855

Calzetti D., Armus L., Bohlin R. C., Kinney A. L., Koornneef J., Storchi-Bergmann T., 2000, ApJ, 533, 682

Egami E., Kneib J.-P., Rieke G., Ellis R., Richard J., Rigby J., Papovich C., Stark D., et al., 2005, ApJ, 618, L5

Ellis R., Santos M. R., Kneib J.-P., Kuijken K., 2001, ApJ, 560, L119

Eyles L. P., Bunker A. J., Ellis R. S., Lacy M., Stanway E. R., Stark D. P., Chiu K., 2007, MNRAS, 374, 910

Finkelstein S., Papovich C., Giavalisco M., Reddy N., Ferguson H., Koekemoer A., Dickinson M., 2010, ApJ, 719, 1250

Hook R., Stoehr F., 2008, WFC3 Support in Tiny Tim. Tech. rep.

Jullo E., Kneib J.-P., Limousin M., Elíasdóttir Á., Marshall P. J., Verdugo T., 2007, New Journal of Physics, 9, 447

Kennicutt R. C., 1998, ApJ, 498, 541

Kneib J.-P., Ellis R. S., Santos M. R., Richard J., 2004, ApJ, 607, 697

Koekemoer A. M., Fruchter A. S., Hook R. N., Hack W., 2002, in The 2002 HST Calibration Workshop, S. Arribas, A. Koekemoer, & B. Whitmore, ed., pp. 337–+

Labbé I., González V., Bouwens R. J., Illingworth G. D., Franx M., Trenti M., Oesch P. A., van Dokkum P. G., et al., 2010, ApJ, 716, L103

Massey R., 2010, MNRAS, 409, L109

McLure R. J., Dunlop J. S., Cirasuolo M., Koekemoer A. M., Sabbi E., Stark D. P., Targett T. A., Ellis R. S., 2010, MNRAS, 403, 960

Meiksin A., 2006, MNRAS, 365, 807

Mobasher B., Dickinson M., Ferguson H., Giavalisco M., Wiklind T., Stark D., Ellis R., Fall S., et al., 2005, ApJ, 635, 832

Newman A. B., Treu T., Ellis R. S., Sand D. J., 2011, ApJ in press, astro-ph/1101.3553

Poggianti B., Bressan A., Franceschini A., 2001, ApJ, 550, 195

Richard J., Pei L., Limousin M., Jullo E., Kneib J. P., 2009, A&A, 498, 37

Richard J., Smith G. P., Kneib J., Ellis R. S., Sanderson A. J. R., Pei L., Targett T. A., Sand D. J., et al., 2010, MNRAS, 404, 325

Richard J., Stark D. P., Ellis R. S., George M. R., Egami E., Kneib J.-P., Smith G. P., 2008, ApJ, 685, 705

Salpeter E. E., 1955, ApJ, 121, 161

Schaerer D., de Barros S., 2010, A&A, 515, A73+

Smith G. P., Edge A. C., Eke V. R., Nichol R. C., Smail I., Kneib J., 2003, ApJ, 590, L79

Smith G. P., Kneib J.-P., Smail I., Mazzotta P., Ebeling H., Czoske O., 2005, MNRAS, 359, 417

Stark D. P., Ellis R. S., Bunker A., Bundy K., Targett T., Benson A., Lacy M., 2009, ApJ, 697, 1493

Stark D. P., Ellis R. S., Chiu K., Ouchi M., Bunker A., 2010, MNRAS, 408, 1628

Stark D. P., Ellis R. S., Ouchi M., 2011, ApJ, 728, L2+

Steidel C. C., Bogosavljević M., Shapley A. E., Kollmeier J. A., Reddy N. A., Erb D. K., Pettini M., 2011, ApJ

submitted, astro-ph/1101.2204